Bladelets – Winglets on Blades of Wind Turbines: A Multiobjective Design Optimization Study

Article *in* Journal of Solar Energy Engineering · May 2019

DOI: 10.1115/1.4043657

4 authors, including:

Sohail R Reddy
Florida International University
27 PUBLICATIONS **105** CITATIONS

SEE PROFILE

George S Dulikravich
Florida International University
350 PUBLICATIONS **3,005** CITATIONS

SEE PROFILE

Helmut Sobieczky
Inst. of Technology Vienna
121 PUBLICATIONS **890** CITATIONS

SEE PROFILE

Sohail R. Reddy
Presidential Fellow
MAIDROC Laboratory,
Department of Mechanical and Materials Engineering,
Florida International University,
Miami, FL 33174
e-mail: sredd001@fiu.edu

George S. Dulikravich
Professor
Fellow ASME
Director of MAIDROC Lab,
MAIDROC Laboratory,
Department of Mechanical and Materials Engineering,
Florida International University,
Miami, FL 33174
e-mail: dulikrav@fiu.edu

Helmut Sobieczky
Professor
Institute of Fluid Mechanics and Heat Transfer,
Vienna University of Technology,
1010 Vienna, Austria
e-mail: helmut@sobieczky.at

Manuel Gonzalez
MAIDROC Laboratory,
Department of Mechanical and Materials Engineering,
Florida International University,
Miami, FL 33174
e-mail: mgonz697@fiu.edu

Bladelets—Winglets on Blades of Wind Turbines: A Multiobjective Design Optimization Study

The work presented in this paper used rigorous 3D flow-field analysis combined with multi-objective constrained shape design optimization for the design of complete blade + bladelet configurations for a three-blade horizontal-axis wind turbine. The fluid flow analysis in this work was performed using Openfoam *software. The 3D, steady, incompressible, turbulent flow Reynolds-Averaged Navier–Stokes equations were solved in the rotating frame of reference for each combination of wind turbine blade and bladelet geometry. The free stream uniform wind speed in all cases was assumed to be 9 m* s^{-1}*. The three simultaneous design optimization objectives were as follows: (a) maximize the coefficient of power, (b) minimize the coefficient of thrust force, and (c) minimize twisting moment around the blade axis. The bladelet geometry was fully defined by using a small number of parameters. The optimization was carried out by creating a multidimensional response surface for each of the simultaneous objectives. The response surfaces were based on radial basis functions, where the support points were designs analyzed using the high-fidelity computational fluid dynamics (CFD) analysis of the full blade + bladelet geometry. The response surfaces were then coupled to an optimization algorithm in mode*frontier *software. The predicted values of the objective functions for the optimum designs were then again validated using* Openfoam *high-fidelity analysis code. Results for a Pareto-optimized bladelet on a given blade indicate that more than 4% increase in the coefficient of power at minimal thrust force penalty is possible at off-design conditions compared to the same wind turbine rotor blade without a bladelet.* [DOI: 10.1115/1.4043657]

1 Introduction

Although much work has been reported on the design of winglets on airplane wings [1,2], the volume of published efforts to design bladelets (winglets at the tips of the wind turbine blades) for rotating lifting surfaces is still very limited. This is especially true for mathematical optimization of bladelets for horizontal-axis wind turbine blades.

In recent years, a strong push toward energy independence and clean, renewable energy has resulted in significant advances in the area of solar, wind, and nuclear energies. In 2015, 11% of energy produced was renewable energy, 19% of which was harvested from the wind. Bazmi and Zahedi [3] stated that the wind power is the second fastest growing renewable energy with an annual growth rate of 34%. Evans et al. [4] showed that the wind power led to lowest greenhouse gas emission, least water consumption, and most favorable social impact than geothermal, hydropower, and solar energy.

For large-scale applications, such as offshore wind farms, horizontal-axis wind turbines (HAWTs) are the preferred choice. Although the wind turbines have become more efficient over the decade, their basic shape has remained unaltered.

Winglets have previously been investigated for their ability to increase the efficiency of the horizontal-axis wind turbines. Wind turbines have previously been extensively studied. Zhao et al. [5] performed computational aerodynamic analysis on upwind and downwind turbine configurations. Wood and Deiterding [6] used a detailed Lattice Boltzmann method to perform a fully 3D turbulent flow analysis of HAWT configurations. Tobin et al. [7] experimentally investigated the effects on winglets on wake and performance of wind turbines. Their work showed an increase in power and thrust coefficients by 8% and 15%, respectively. Gaunaa and Johansen [8] numerically investigated the aerodynamic efficiency of turbine rotors with winglets. They reported that the increase in power is due to the reduction of tip losses and is not connected with a downwind shift of wake vorticity. Gertz et al. [9] experimentally investigated the effects of wind speeds and rotor rotation speeds on power production. Ferrer and Munduate [10] used computational fluid dynamics (CFD) analysis to carry out a blade tip comparison study. To the authors' knowledge, a multi-objective optimization study of the bladelet configuration has never been published before. This is an extension of the work presented in Ref. [11]. Only recently, Zahle et al. [12] performed a wingtip optimization for wind turbine blades and achieved an increase in efficiency of 2.6%.

2 Analysis

2.1 Geometry Definition. The standard Vestas27 wind turbine blade geometry [13] of a $R_{rotor} = 13.5$ m radius rotor was used as the benchmark in this work. Different bladelets were virtually added to the tip of the Vestas27 blade. Only bladelet shapes were optimized, while the blade geometry was kept unchanged.

An efficient manner for representing geometry is needed in order to minimize the number of variables that the optimization algorithm will have to use. Defining the geometry with an inadequate number of parameters leads to a restricted design space for the multi-

Contributed by the Solar Energy Division of ASME for publication in the Journal of Solar Energy Engineering: Including Wind Energy and Building Energy Conservation. Manuscript received May 26, 2018; final manuscript received April 24, 2019; published online May 20, 2019. Assoc. Editor: Douglas Cairns.

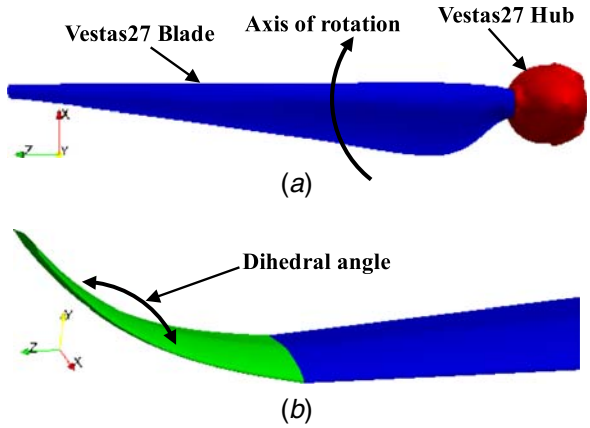

Fig. 1 (*a*) Geometry for baseline Vestas27 wind turbine blade and (*b*) a sketch of a bladelet at the tip of the Vestas27 blade

objective optimizer. Conversely, defining the geometry with excessive number of design variables leads to an over sensitive design and often wastes computational resources.

Each bladelet configuration in this study was defined using five variables: bladelet span, twist angle, dihedral angle, sweep angle, and taper ratio. The axis about which the twist angle is defined is taken as the vector, normal to the airfoil cross section. The dihedral angle is shown in Fig. 1(*b*). The taper ratio is the ratio of the bladelet tip chord to the bladelet root chord. Figure 1 shows the Vestas27 blade used in this study and a typical bladelet configuration. Details of the Vestas27 geometry are given in Ref. [13]. The dihedral angle was defined as a second-order polynomial to satisfy continuity conditions at the bladelet root and the blade tip. All other parameters were chosen to vary linearly as a function of bladelet span. The ranges for each of the geometric parameter are shown in Table 1.

2.2 Mathematical Model. The five parameters in Table 1 were selected as the design parameters that need to be optimized. The three simultaneous objectives were to maximize the coefficient of rotor power [14] and to minimize the coefficients of twisting moment and thrust coefficient. The coefficient of rotor power, C_P, is defined as follows:

$$C_P = \frac{P_{rotor}}{0.5\rho_\infty V_\infty^3 R_{rotor}^2 \pi} \tag{1}$$

The coefficient of rotor axial thrust force T_{rotor} is defined as follows [13]:

$$C_T = \frac{T_{rotor}}{0.5\rho_\infty V_\infty^2 R_{rotor}^2 \pi} \tag{2}$$

Here, P_{rotor} is the power extracted by the wind turbine rotor (three blades together in this test case), which can be calculated as follows:

$$P_{rotor} = M\Omega \tag{3}$$

Here, M is the torque around the rotor axis generated by the rotor and Ω is the angular speed of the rotor.

The mass and momentum conservation equations for 3D, incompressible, viscous, turbulent flow in a rotating frame of reference can be expressed in a vector operator form as

$$\nabla \cdot \vec{V}_a = 0 \tag{4}$$

$$(\vec{V}_r \cdot \nabla)\vec{V}_r = -\frac{\nabla p}{\rho} + (\mu_\ell + \mu_t)\nabla^2 \vec{V}_a - \vec{\Omega} \times (2\vec{V}_r - \vec{\Omega} \times \vec{r}) \tag{5}$$

$$\vec{V}_a = \vec{V}_r + \vec{\Omega} \times \vec{r} \tag{6}$$

Here, $\vec{\Omega}$ is the steady angular velocity of the wind turbine rotor, μ_ℓ and μ_t are dynamic viscosity coefficients for laminar and turbulent flows, respectively, $\vec{V}_r$ is the velocity relative to the blade, $\vec{V}_a$ is the absolute velocity, $\vec{r}$ is the position vector in the rotor plane, ρ is the density of air, and p is local air pressure.

Table 1 Allowable range and step size for each geometric design variable used to define the bladelet configurations

	Minimum	Maximum	Step size
Span (m)	0.1	1.5	0.1
Twist angle (deg)	−20.0	20.0	1.0
Dihedral angle (deg)	−45.0	45.0	1.0
Sweep angle (deg)	−45.0	45.0	1.0
Taper ratio	0.1	1.0	0.1

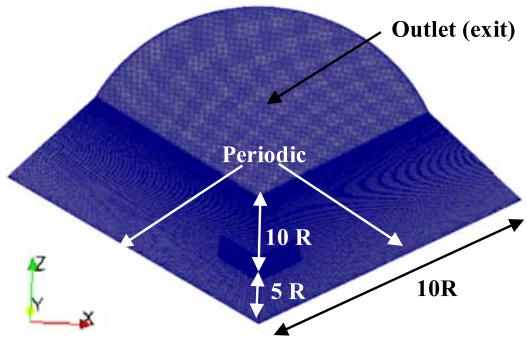

Fig. 2 Dimensions of the computational domain used to analyze each blade + bladelet geometry

2.3 Computational Analysis. The computational grid of hexahedral cells for each candidate blade + bladelet configuration was generated using cfMesh [15]. A total of ten layers of grid cells were placed within the viscous sublayer. Figure 2 shows the relative dimensions of the computational domain, where R is the rotor radius. Only one-third of the entire wind turbine configuration was analyzed due to the circumferential periodicity of the geometry. Each configuration was analyzed for the uniform axial free stream air speed of $V = 9$ m s^{-1} with the rotor rotating at $\Omega = 12$ rpm.

The flow-field governing equations were solved using finite volume method on a hybrid computational grid with 12 million grid cells arrived at using a mesh convergence study. The utilized flow-field analysis software OpenFOAM[1] was validated on the benchmark NREL 5-MW baseline wind turbine by Zhao et al. [16] and Stergiannis et al. [17]. The κ-ω-shear stress transport (SST) turbulence model proposed by Menter [18] was employed to model turbulence. The κ-ω-SST was extensively utilized in the simulation of wind turbine aerodynamics with results being in good agreement with experiments [16,17]. Each analysis was run on Intel® Xeon® CPU E7-8860 v4 @ 2.20 GHz processors and took approximately 22 h.

Table 2 shows C_P for the Vestas27 rotor from the calculations using the Lattice Boltzmann method [6] and from experimental measurements [13] for a tip speed ratio of 5.84. The geometry in both of these works featured wind turbine tower and ground effects, both of which are not considered in this work. It can be seen that the numerical scheme used in this work accurately computes the turbine power, thereby validating its use in the multi-objective design optimization.

2.4 Aerodynamic Analysis of Vestas27 Blade. As the performance benefits of various bladelet configurations are being analyzed, a benchmark case is needed for comparison. For this reason, the Vestas27 blade aerodynamic performance was analyzed using OpenFOAM software[2] at an off-design freestream velocity of 9 m s^{-1} rotating at 12 rpm. Relative airspeed and pressure on the

[1] https://openfoam.org
[2] See Note 1.

Table 2 Comparison of the power coefficients for Vestas27 turbine at on-design conditions obtained using various methods

	Experiment [11]	Lattice Boltzmann [6]	Present work
C_P	0.459	0.440	0.468
C_P error (%)	—	−4.1	+1.9

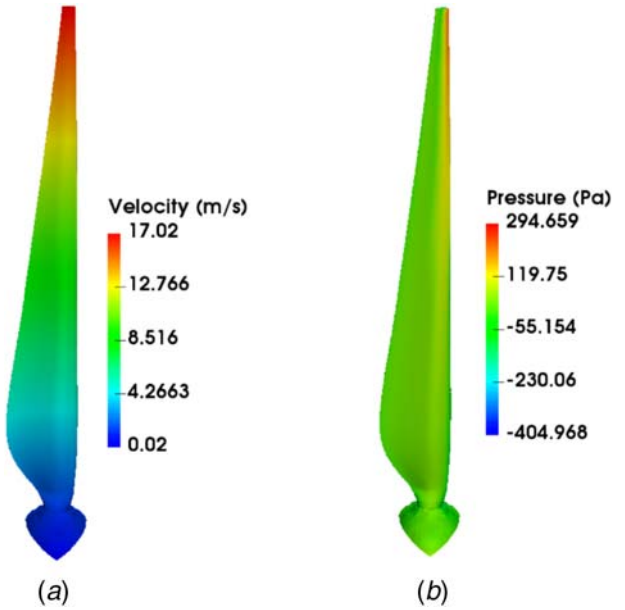

Fig. 3 Results from OpenFOAM aerodynamic analysis: (*a*) relative velocity and (*b*) pressure field on the surface of the Vestas27 blade without a bladelet

Table 3 Objective function values for the benchmark Vestas27 blade without a bladelet (C_M is aerodynamic twisting moment)

C_P	C_T	C_M
0.154	0.174	0.028

surface of the blade are shown in Fig. 3. Relative airspeed computed at the blade tip using Eq. (6) for a rotor radius of the Vestas27 blade $R_{rotor} = 13.5$ m matched as expected with the blade tip airspeed obtained from the OpenFOAM software. The values of the three coefficients (objective functions) for this benchmark are given in Table 3.

2.5 Aerodynamic Analysis of Vestas27 Blade With Unoptimized Bladelet. For comparison purposes, the Vestas27 turbine with unoptimized bladelets was also analyzed under off-design operating conditions of $V = 9$ m s^{-1} and $\Omega = 12$ rpm. Table 4 shows the three calculated performance coefficients.

Comparison with Table 3 indicates that even unoptimized bladelets can slightly improve the wind turbine performance. Figure 4 shows the relative velocity field and the pressure field on the Vestas27 blade with an unoptimized bladelet.

3 Multi-Objective Optimization

The optimization objective function values for each blade + bladelet configuration were obtained by performing a full 3D, turbulent

Table 4 Objective function values for the benchmark Vestas27 turbine rotor having blades with unoptimized bladelets

C_P	C_T	C_M
0.156	0.182	0.030

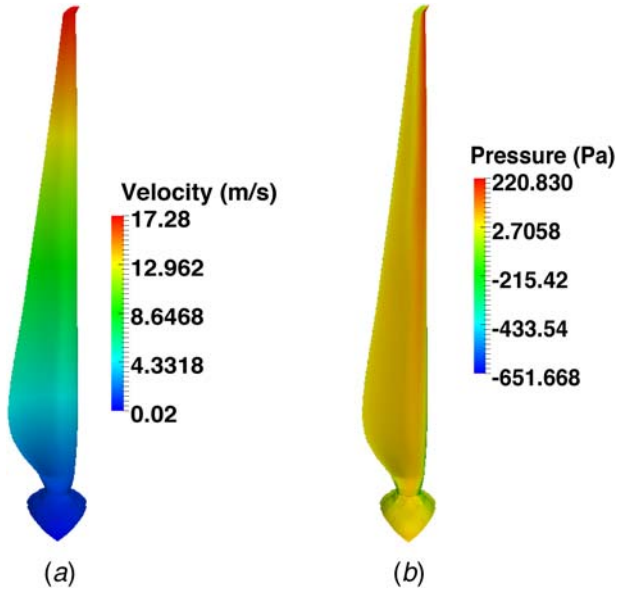

Fig. 4 (*a*) Relative velocity and (*b*) pressure field on the surface of the Vestas27 blade with an unoptimized bladelet

fluid flow analysis using the OpenFOAM software.[3] The built-in solver MRFSimpleFoam was used to simulate the wind turbine configuration in a rotating frame of reference.

It should be pointed out that this study did not involve shape optimization of the blade. An unchanged shape of the rotor blade was used together with the bladelet when optimizing the bladelet shape and size. This study did not involve simultaneous shape optimization of both the blade and the bladelet. The multi-objective optimization of the bladelet configuration was carried out using the commercial software package modeFRONTIER [19].

Because the computational time for each analysis is so large, an alternative, much faster method is required to compute the thousands of objective function values (coefficients of rotor power, thrust force, and twisting moment) needed by the optimization process. For this reason, surrogate models were used to obtain the objective function values for each blade + bladelet configuration. A response surface based on Hardy's multiquadrics radial basis functions [20] was created for each of the three objectives. It is well known that the accuracy of the response surface is greatly influenced by the distribution of the support points used to construct it. For this reason, an initial population of 50 candidate designs (blade + bladelet configurations) were created using SOBOL's [21] pseudo-random number generator that uniformly distributed the candidate values of the five design variables (Table 1) within the five-dimensional design space. Figure 5 shows the optimization methodology implemented in this work.

All three response surfaces were coupled to the NSGA-II [22] multi-objective optimization algorithm to search the design and

[3]See Note 1.

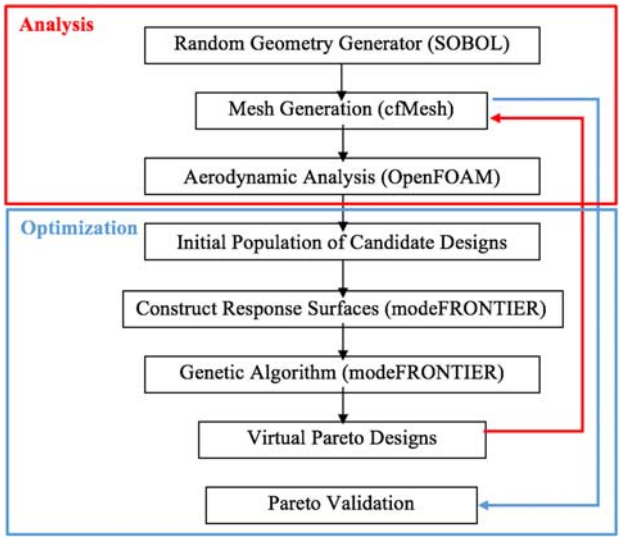

Fig. 5 Workflow of the optimization framework

objective function space for Pareto optimal designs. The optimizer was initialized with a population size of 100 and was ran for 100 generations. The crossover and mutation distribution indices were both set at 20. The crossover and mutation probabilities were set at 0.9 and 0.2, respectively.

The maximum allowable coefficient of power was limited to the Betz limit of 0.5925 to limit search to the feasible domain.

From three five-dimensional response surfaces, the NSGA-II optimization algorithm was able to find other wind turbine bladelet designs that perform better than the initial population of 50 shapes (Fig. 6). Due to conflicting objectives, the multi-objective optimization algorithm arrives at a Pareto frontier of best trade-off solutions rather than a single global optimum.

Because the accuracy of the response surface deteriorates in regions within and outside the design space, four virtual bladelet configurations were selected at random from the Pareto frontier and analyzed using OpenFOAM. The objective function values obtained by the optimizer from the response surfaces deviated at most by 3% from the ones obtained from the CFD analysis.

The five design parameters of the four virtual Pareto-optimized designs were than randomly perturbed by 2% to simulate defects due to manufacturing tolerance in an effort to study the sensitivity of the designs. The design parameters of the least-sensitive combination of the unoptimized wind turbine blades + optimized bladelets are given in Table 5.

Figure 7 shows the unoptimized and optimized bladelets.

Figure 8 shows the velocity and pressure fields on the surface of the unoptimized blade with the optimized bladelet.

The range of increase in the coefficient of power due to the addition of optimized bladelets is in good agreement with the results presented in other studies [8,9]. The addition of the optimized bladelet resulted in a 4.5% increase in C_P and 0.0% decrease in the blade twisting moment, while increasing the coefficient of axial thrust force by 4.0%.

The Vestas27 blade, both with and without bladelet, is simulated for a range of operating conditions. The Vestas27, being an older model, is a fixed speed wind turbine meaning that the rotor speed is constant. Figure 9 shows the variation of the coefficient of power with varying tip speed ratio and with varying wind speed.

Both figures demonstrate that the numerical solver used in this work is in good agreement with the experimental data. The maximum error is 5%. It also shows that the addition of a bladelet leads to a slight increase in the power coefficient with a maximum increase of 5%. It should be mentioned that the bladelet was not optimized for this operating range and that a further increase in

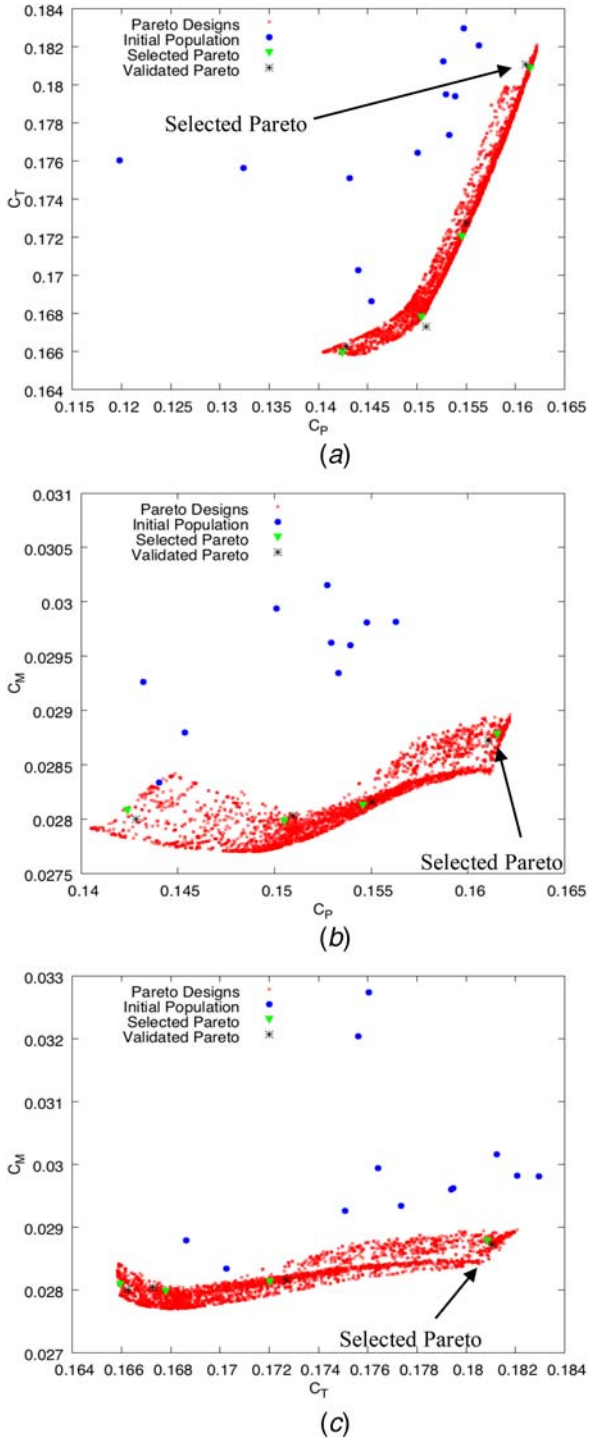

Fig. 6 Response surface points for (*a*) C_T *versus* C_P, (*b*) C_M *versus* C_P, and (c) C_M *versus* C_T

Table 5 Pareto-optimized values of the five design variables and objective functions of the Pareto-optimized configuration

Span (m)	0.8
Twist angle	−9.0
Dihedral angle	23.0
Sweep angle	23.0
Taper ratio	0.7
C_P, ΔC_P %	0.161, +4.5
C_T, ΔC_T %	0.181, +4.0
C_M, ΔC_M %	0.028, 0.0

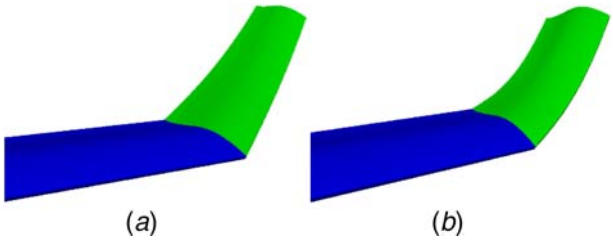

Fig. 7 (*a*) Unoptimized and (*b*) optimized bladelets

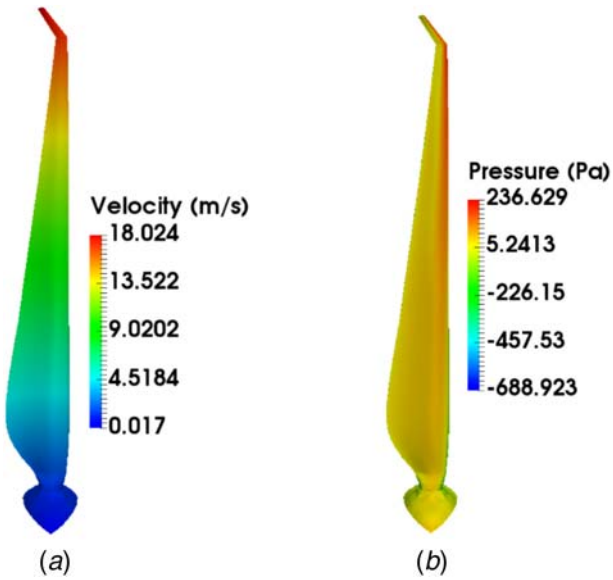

Fig. 8 (*a*) Relative velocity and (*b*) pressure field on the surface of the unoptimized blade + optimized bladelet configuration

the power coefficient is possible if optimized for a range of operating conditions.

4 Conclusion

This work investigated the effectiveness of bladelets placed on the tips of wind turbine blades on increasing wind turbine rotor power output. Aerodynamics of each blade + bladelet 3D configuration was analyzed using the OpenFOAM solver, MRFSimpleFoam. Multi-objective optimization was performed on the bladelet configuration only (not on the blade configuration) using modeFRONTIER software. The shape of each bladelet configuration was defined by the span, sweep angle, dihedral angle, twist angle, and the taper ratio. The three simultaneous objectives were to maximize the coefficient of power, while minimizing the coefficient of thrust and the coefficient of blade twisting moment around its stacking axis. A constraint of the Betz limit was placed on the maximum allowable power coefficient.

A multidimensional response surface based on radial basis functions was created for each of the three objectives and coupled with the NSGA-II optimization algorithm to arrive at a Pareto frontier. Four virtual Pareto designs were selected at random from the Pareto frontier and validated in OpenFOAM. Of the four selected designs, the Pareto design, which is least sensitive to geometric defects, is presented.

It was demonstrated that bladelets can increase the power output of the wind turbine rotor and that the proposed multi-objective optimization framework is capable of identifying several candidate blade + bladelet configurations in the multidimensional design space. It is expected that even higher performance of a blade + bladelet combination is possible if both blade and the bladelet shapes are optimized together, if more complex bladelet shapes are considered and if more accurate response surfaces are used having more support points.

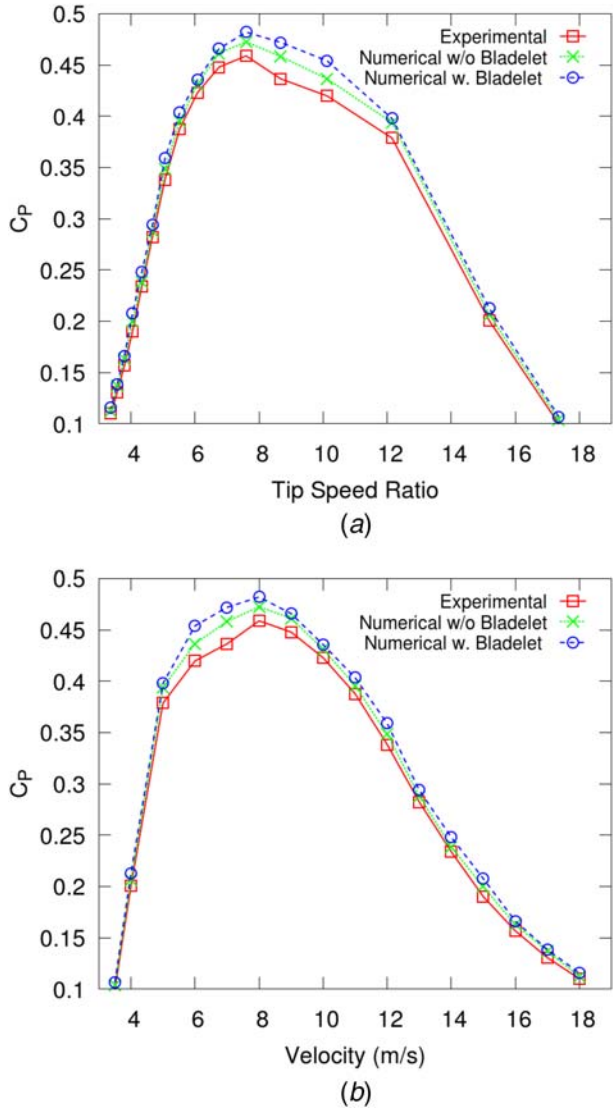

Fig. 9 Variation of the coefficient of power as a function of (*a*) the tip speed ratio and (*b*) velocity

Acknowledgment

The lead author gratefully acknowledges the financial support from Florida International University in the form of an FIU Presidential Fellowship and FIU Dissertation Year Fellowship. The authors would also like to express their appreciation to Professor Carlo Poloni, founder and president of ESTECO, for providing modeFRONTIER optimization software free of charge for this project. They are also grateful for the blade geometry and flow-field analysis data obtained using the Lattice Boltzmann method provided by Dr. Stephen Wood.

References

[1] Gavrilovic, N. N., Rasuo, B. P., Dulikravich, G. S., and Parezanovic, V., 2015, "Commercial Aircraft Performance Improvement By Using Winglets," FME Trans., **43**(1), pp. 1–8.

[2] Reddy, S. R., Sobieczky, H., Dulikravich, G. S., and Abdoli, A., 2016, "Multi-Element Winglets: Multi-Objective Optimization of Aerodynamic Shapes," AIAA J. Aircraft, **5**(4), pp. 992–1000.
[3] Bazmi, A. A., and Zahedi, G., 2011, "Sustainable Energy Systems: Role of Optimization Modeling Techniques in Power Generation and Supply—A Review," Renew. Sustain. Energ. Rev., **15**(8), pp. 3480–3500.
[4] Evans, A., Strezov, V., and Evans, T. J., 2009, "Assessment of Sustainability Indicators for Renewable Energy Technologies," Renew. Sustain. Energ. Rev., **13**(5), pp. 1082–1088.
[5] Zhao, Q., Sheng, C., and Afjeh, A., 2014, "Computational Aerodynamic Analysis of Offshore Upwind Downwind Turbines," J. Aerodyn., **2014**, p. 860637.
[6] Wood, S. L., and Deiterding, R., 2015, "A Lattice Boltzmann Method for Horizontal Axis Wind Turbine Simulation," 14th International Conference on Wind Engineering, Porto Alegre, Brazil, June 21–26, pp. 1–18.
[7] Tobin, N., Hamed, A. M., and Chamorro, L. P., 2015, "An Experimental Study on the Effects of Winglets on the Wake and Performance of a Model Wind Turbine," Energies, **8**, pp. 11955–11972.
[8] Gaunaa, M., and Johansen, J., 2007, "Determination of the Maximum Aerodynamic Efficiency of Wind Turbine Rotors With Winglets," J. Phys. Conf. Ser., **75**, pp. 1–12.
[9] Gertz, D., Johnson, D. A., and Swytink-Binnema, N., 2012, "An Evaluation Testbed for Wind Turbine Blade Tip Designs—Winglet Results," Wind Eng., **36**(4), pp. 389–410.
[10] Ferrer, E., and Munduate, X., 2007, "Wind Turbine Blade Tip Comparison Using CFD," J. Phys. Conf. Ser., **75**, pp. 1–10.
[11] Reddy, S. R., Dulikravich, G. S., and Sobieczky, H., 2017, "Bladelets-Winglets on Blades of Wind Turbines: A Multiobjective Design Optimization Study," International Mechanical Engineering Congress and Exposition (IMECE2017-70220), Tampa, FL, Nov. 3–9.
[12] Zahle, F., Sorensen, N. N., McWilliam, M. K., and Barlas, A., 2018, "Computational Fluid Dynamics-Based Surrogate Optimization of Wind Turbine Blade Tip Extension for Maximizing Energy Production," J. Phys. Conf. Ser., **1037**, p. 042013.
[13] Vestas, 1994, "Vestas V27-225kW, *50 Hz Wind Turbine With Tubular/Lattice Tower Item no.: 941129 Version 1.2.0.24*," Vestas, Aarhus, Denmark.
[14] Burton, T., Sharpe, D., Jenkins, N., and Bossanyi, E., 2001, *Wind Energy*, John Willey & Sons Book Co., Chichester, England.
[15] Juretic, F., 2015, "*cfMesh User Guide*," version 1.1, Creative Fields, Ltd., London.
[16] Zhao, W., Cheng, P., and Wan, D., 2014, "Numerical Computation of Aerodynamic Performances of NREL Offshore 5-MW Baseline Wind Turbine," Proceedings of the Eleventh Pacific/Asia Offshore Mechanics Symposium, Shanghai, China, Oct. 12–16, pp. 13–18.
[17] Stergiannis, N., Lacor, C., Beeck, J. V., and Donnelly, R., 2016, "CFD Modelling Approaches Against Single Wind Turbine Wake Measurements Using RANS," J. Phys. Conf. Ser., **753**, pp. 1–16.
[18] Menter, F., 1994, "Two Equation Eddy-Viscosity Turbulence Models for Engineering Applications," AIAA J., **32**(8), pp. 1598–1605.
[19] modeFRONTIER, 2014, "Software Package, Ver. 4.5.4," ESTECO, Trieste, Italy.
[20] Colaco, M. J., and Dulikravich, G. S., 2011, "A Survey of Basic Deterministic, Heuristic and Hybrid Methods for Single-Objective Optimization and Response Surface Generation," *Thermal Measurements and Inverse Techniques*, H. R. B. Orlande, O. Fudym, D. Milet, and R. Cotta, eds., Taylor and Francis, Philadelphia, PA, pp. 355–405, Chapter 10,
[21] Sobol, I. M., 1967, "Distribution of Points in a Cube and Approximate Evaluations of Integrals," U.S.S.R. Comput. Math. Math. Phys., **7**, pp. 86–112.
[22] Deb, K., Pratap, A., Agarwal, S., and Meyarivan, T., 2002, "A Fast and Elitist Multiobjective Genetic Algorithm: NSGA-II," IEEE Trans. Evol. Comput., **6** (2), pp. 182–197.